International Journal of Mining and Geo-Engineering

IJMGE

IJMGE 52-2 (2018) 177-185

DOI: 10.22059/ijmge.2018.223076.594649

Application of Committee machine with particle swarm optimization in assessment of permeability based on thin section image analysis

Mahnaz Abedini [a], Mansour Ziaii [a, *] and Javad Ghiasi-Freez [b]

[a] *Faculty of mining, petroleum and geophysics, Shahrood university of technology, Iran*

[b] *Iranian Central Oil Fields Company (ICOFC), Subsidiary of National Iranian Oil Company (NIOC) Tehran, Iran*

Article History:

Received: 27 December 2016,

Revised: 13 August 2017,

Accepted: 03 February 2018.

ABSTRACT

Permeability is the ability of a porous rock to transmit fluids and is one of the most important properties of a reservoir rock because the oil production depends on reservoirs permeability. Permeability is determined using a variety of methods that are usually expensive and time consuming. Analyzing the properties of a reservoir rock with image analysis and intelligent systems saves time and money. This study presents an improved model based on the integration of petrographic data and intelligent systems to predict the permeability. Petrographic image analysis was employed to measure the types of porosity including intergranular, intragranular, moldic, micro and optical, as well as the amount of cement, limestone, dolomite and anhydrite, the types of texture and the mean geometrical shape coefficient of pores. Permeability was first predicted using the three individual intelligent systems including neural network (NN), fuzzy logic (FL), and neuro-fuzzy (NF) models, respectively. The mean squared error (MSE) of the NN, FL and NF methods are 0.0107, 0.0081 and 0.0080, which correspond with R^2 values of 0.8830, 0.9193 and 0.9136, respectively. Afterward, two types of committee machines were used with intelligent systems (CMIS) to combine the predicted values of permeability from individual intelligent systems: simple averaging (SA) and weighted averaging (WA). In the WA, a particle swarm optimization (PSO) was employed to obtain the optimal contribution of each intelligent system. The MSE of the CMIS-SA and CMIS-WA were 0.0072 and 0.0066, which correspond with R^2 values of 0.9262 and 0.9260, respectively. These show that the CMIS-WA performed better than the NN, FL, and NF models individually. In addition, a multiple linear regression (MLR) was used to compare the results with the other techniques. The R^2 value between the core and MLR permeability is 0.8699. Therefore, the integration of petrographic data and intelligent systems provided more accurate results than the MLR model.

Keywords : *Committee machine, Image analysis, Optimization, Particle swarm, Permeability*

1. Introduction

Permeability is one of the most significant petrophysical characteristics of reservoir rocks. There are many approaches to measure the permeability. Laboratory measurement and well-equipped testing approaches are not only time consuming, but also very expensive.

Intelligent systems are suitable alternative approaches to assess the permeability with a high accuracy and without wasting time and money [1-5]. Employing the image analysis is another way to predict the permeability. Simple models such as Kozeny-Carman predicted the permeability using the extracted porosity and specific surface areas from image analysis. Several researchers have used this method for sandstone formations [6-10].

Koskun et al. (1993) proposed a simple method for estimating the permeability using the data derived from image analysis of thin sections [11]. Anselmetti et al. (1998) used an artificial neural network model to analysis the sensitivity of petrographic data in permeability assessment [12]. Ali and Chawathe (2000) used a neural net because of its ability to learn the non-linear relationships between multiple input and output variables [13]. Egmont-Peterson et al. (2000) reviewed more than 200 applications of neural networks in image analysis [14]. Hatfield and Granham (2001) used image analysis to improve the permeability prediction. They obtained a stronger relationship in the permeability-porosity plot where the image porosity was used rather than the plug porosity [15]. Lock et al. (2002) developed a model to predict the permeability based on image analysis of its pore structure [16]. Zimmerman et al. (2007) presented a model based on image analysis to predict the permeability from sedimentary core samples [17]. Wieling (2013) developed a routine to analyze the images. Image analysis was based on the RGB color data and its auto-covariance properties, to enable mapping the color and texture of a core. The results of this image analysis was used to classify the core, based on lithology and grain size, and produce a permeability model for the core [18]. Blunt et al. (2013) reviewed the pore-scale imaging and modeling, and presented a methodology to predict flow and transport properties including permeability. In addition, they compared the predicted relative permeability with core-scale measurements [19]. Saxena et al. (2017) presented a new approach for predicting the permeability using thin sections. Their approach involved two steps: computing the permeability of thin sections and application of new 2D-3D transforms that connect the permeability of a thin section to the 3D rock permeability using calibration parameters. They proposed to, first, calibrate the proposed models using the available 3D information on the rock microstructure, and then, predict the permeability of rock from the same geological formation for which only 2D thin sections are available [20].

A committee machine has a parallel structure that combines the obtained results from individual experts using an optimization technique and enhances the accuracy of final model [21, 22]. In recent years, committee machine with intelligent systems have been applied to

* Corresponding author. *E-mail address:* mziaii@shahroodut.ac.ir (M. Ziaii).

predict reservoir characteristics [23-28]. Ghiasi-Freez et al. (2012) used two committee machines to improve the accuracy of flow unit prediction [29].

Particle swarm optimization (PSO) is one of these optimization methods. Implementation of PSO is easy. This algorithm has been successfully applied in many areas, such as function optimization.

PSO has used to solve various problems and analyses [30-33]. Shi and Eberhart (1999) empirically studied the performance of PSO. They illustrated that PSO always converged very quickly toward the optimal positions but might slow its convergence speed near the minimum [34]. Coello (2004) used PSO in order to handle the problems with several objective functions. The result indicates that PSO is highly competitive and can be considered as a viable alternative to solve multi objective optimization problems [35]. Poli et al. (2007) comprised a snapshot of PSO from the authors' perspective, including variations in the algorithm, current researches, applications and ongoing problems [36]. Ahmadi et al. (2013) implemented a neural network model to forecast the permeability of a reservoir. Then, they used a hybrid genetic algorithm and the PSO method to optimize the neural network model. They compared the results from the hybrid method with that of the conventional neural network. The comparison demonstrated the usefulness of the developed hybrid genetic algorithm and PSO in predicting the reservoir permeability [37].

This methodology was applied to integrated different intelligent systems and petrographic image analysis with the committee machine for permeability prediction with an example from the South Pars Gas Field. In addition, the results were compared with the MLR model.

2. Geology of the South Pars Gas Field

In the South Pars Gas Field, the occurrence of gas is mostly limited to the Dalan and Kangan Formations. The Dalan and Kangan formations have four main beds K_1, K_2, K_3 and K_4 [38]. The Dalan Formation formed in the late Permian. This Formation is more than 680 meters thick and consists of limestone and dolomite. The Kangan Formation formed in early Triassic. In the South Pars Gas Field, this Formation is 193 meters thick. The Kangan Formation overlies the Dalan Formation [39]. In this study, the core data and thin sections of the Kangan and Dalan Formations were examined.

3. Theory and methodology

3.1. Image analysis

Image analysis is an introduction to machine vision. Machine vision is a tool for pattern recognition. In image analysis, specified parameters are separated a particular object from the rest. Image analysis is conduced as follows: taking the images from saturated thin sections with a blue-dyed epoxy, segmentation, extracting the geometric and petrographic parameters, and pattern recognition.

Segmentation is a process that partitions an image into multiple regions. The best results of segmentation are generally obtained using an RGB colored model. The objective is to segment the object of a specified color (blue) in an RGB color [40].To specify the pixels related to the pores, the intensity of red and green colors are below 203 and the intensity of the blue color trespasses 170. All pixels with the mentioned red, green and blue intensities are converted to a unique blue and the remaining pixels become white. This blue-white image is a three-dimensional one in which every pixel includes three components of red, green and blue. The three-dimensional image is converted into a two-dimensional or a binary image. In a binary image, pores are shown by black pixels (zero) and other parts of the image are defined by white pixels (one).

3.2. Intelligent systems

Intelligent systems have parameters that need to be optimized. Back propagation is a common method of supervised training artificial neural networks. It calculates the gradient of a loss function with respect to all weights in the network. Back propagation requires a desired output for each input value in order to calculate the gradient of loss function.

Then, the error is back propagated through the net and the weights are adjusted during the iterations. The training stops when the best approximations of desired values are calculated [41].

Zadeh introduced the theory of fuzzy in 1965 [42]. This theory is an extension of traditional Boolean logic. Fuzzy logic explains the chance of an event occurrence. The main part of the fuzzy logic is the fuzzy interference system (FIS), which formulates inputs to an output. Mamdani and Assilian (1975) introduced the first type of FIS and Takagi and Sugeno (1985) initiated the second one [43, 44]. Both FISs attempt to control a system by integrating a set of linguistic control roles while the main difference between the methods is an output membership function, which is constant for the Takagi-Sugeno FIS (TS-FIS). In the TS-FIS, a clustering process defines membership functions. Each of the clusters refers to a membership function to generate the if-then rules. The fuzzy system makes a sum of all parts and uses a defuzzification method to find the final outputs.

The Neuro-fuzzy system is one of the most powerful tools that utilizes the advantages of both an artificial neural network and the fuzzy logic. A curved relationship maps the input values on an internal of [0, 1], which is called fuzzification of input values through the membership function. Then, an algorithm such as back propagation or least squares is used to train the membership functions. In a similar way with the fuzzy logic, conditional (if-then) statements are determined in order to train the system, finally.

3.3. Particle swarm optimization

Particle swarm optimization (PSO) is a population-based stochastic optimization technique developed by Eberhart and Kennedy (1995), inspired by social behavior of bird flocking or fish schooling [45]. The system is initialized with a population of random solutions and searches for optima by updating the generations. In PSO, the potential solutions, called particles, fly through the problem space by following the current optimum particles.

Each single solution is a "bird" in the search space. It is called "particle". All of particles have fitness values that are evaluated by the fitness function to be optimized, and have velocities which direct the flying of the particles. In every iteration, each particle is updated by the following two "best" values. The first one is the best ever achieved solution (fitness). The fitness value is stored, as well This value is called pbest. Another "best" value that is tracked by the particle swarm optimizer is the best value obtained so far by any particle in the population. This best value is a global best and called gbest. When a particle takes part of a population as its topological neighbors, the best value is a local best and is called lbest. After finding the two best values, the particle updates its velocity and positions with the following equation:

$$V_i(t) = w \times v_i(t-1) + c_1 \times rand_1 \times \left(P_{i.best} - x_i(t-1)\right) + c_2 \times rand_2 \times \left(P_{g.best} - x_i(t-1)\right) \quad (1)$$

$$x_i = x_i(t-1) + v_i(t) \quad (2)$$

$V_i(t)$ is the particle velocity, $x_i(t-1)$ is the current particle (solution). $P_{i.best}$ and $P_{g.best}$ are defined as stated before. $rand_1$ and $rand_2$ is a random number between (0,1). c_1 and c_2 are learning factors. Usually, $c_1 = c_2 = 2$.

Particles' velocities on each dimension are clamped to a maximum velocity V_{max}. If the sum of accelerations cause the velocity on that dimension to exceed V_{max}, which is a parameter specified by the user, then, the velocity on that dimension would limit to V_{max}.

3.4. Committee machine

A committee machine with intelligent systems (CMIS) was constructed to improve the performance of the intelligent systems. The inputs of a CMIS are the outputs of the individual intelligent systems. A CMIS combines the outputs of the individual models and thus reaps the advantage of all used intelligent systems. A CMIS is created, which has a better performance than the intelligent models.

A CMIS could be constructed in two ways: simple averaging and weighted averaging. In the simple averaging, each single expert has an equal contribution in constructing the CMIS. The weighted averaging method uses an optimization technique to determine the suitable contributions of the individual models in constructing the CMIS.

3.5. Multiple linear regression

Multiple linear regression (MLR) is the most common form of the linear regression analysis. As a predictive analysis, MLR is used to explain the relationship between one continuous dependent variable and two or more independent variables. The population regression line for k explanatory variables [x_1, x_2, ..., x_k] is defined to be equation (3).

$$Y = 0 + 1X_1 + 2X_2 + \cdots + kX_k \quad (3)$$

MLR involves finding the best-fitting surface of a suitable functional form that connects the values of explanatory variables, [X_1, ..., X_k], and the mean value of a response variable, Y, given the values of [X_1, ..., X_k] [46]. The observed values for Y vary about their mean Y and are assumed to have the same standard deviation. The fitted values [b_0, b_1, ..., b_k] estimate the parameters 0, 1, ..., k of the population regression line.

4. Data preparation and input selection

Thin section analyses of one of the wells of the South Pars Gas Field were used for construction and evaluation of the intelligent systems. Data normalization could be done for better prediction of the outputs. In the training data, permeability ranges from 0.1 to 209 md; this wide range causes a low performance of the model in prediction of the permeability. Therefore, the normalized data were used to enhance the performance of prediction. To obtain the petrographic data, 115 thin sections were analyzed, of which, 85 and 30 samples were the training and test data, respectively. Through petrographic image analyses, 11 petrographic elements were acquired for each sample. They include optical porosity, intergranular porosity, intragranular porosity, moldic porosity, and micro porosity, as well as the amount of cement, limestone, dolomite and anhydrite, the types of texture and the mean geometrical shape coefficient of pores.

The obtained parameters from the petrographic image analysis were integrated with the measured permeability to provide the input-output pairs of intelligent models.

For appropriate input selection, the correlation between the permeability versus petrographic results was studied. (Cross plots shown in fig. 1).

The cross plots illustrated that more accurate predictions were obtained through the stronger relationship. Considering the correlation coefficients, the interparticle porosity, the mean geometrical shape coefficient and the types of texture show a stronger correlation with the cores permeability (Table 1). Reduction of the number of inputs to the most significant ones, improved the performance of intelligent systems.

5. Case study

5.1. Neural network

A simple three-layered feed forward neural network was used. The NN model was trained using the Levenberg-Marquardt back propagation algorithm. The Levenberg-Marquardt optimization was used for updating the weights and bias values of the back propagation algorithm. The hidden layer included four neurons. The transfer function between layer 1 and layer 2 was Log-Sigmoid, while Purelin was employed between layer 2 and layer 3 (Table 2). Feedforward networks often have hidden layers of sigmoid neurons followed by an output layer of linear neurons. A layer of neurons with a nonlinear transfer function allows the network to learn nonlinear and linear relationships between the input and output. The linear output layer lets the network produce the values outside the range -1 to +1 [47].

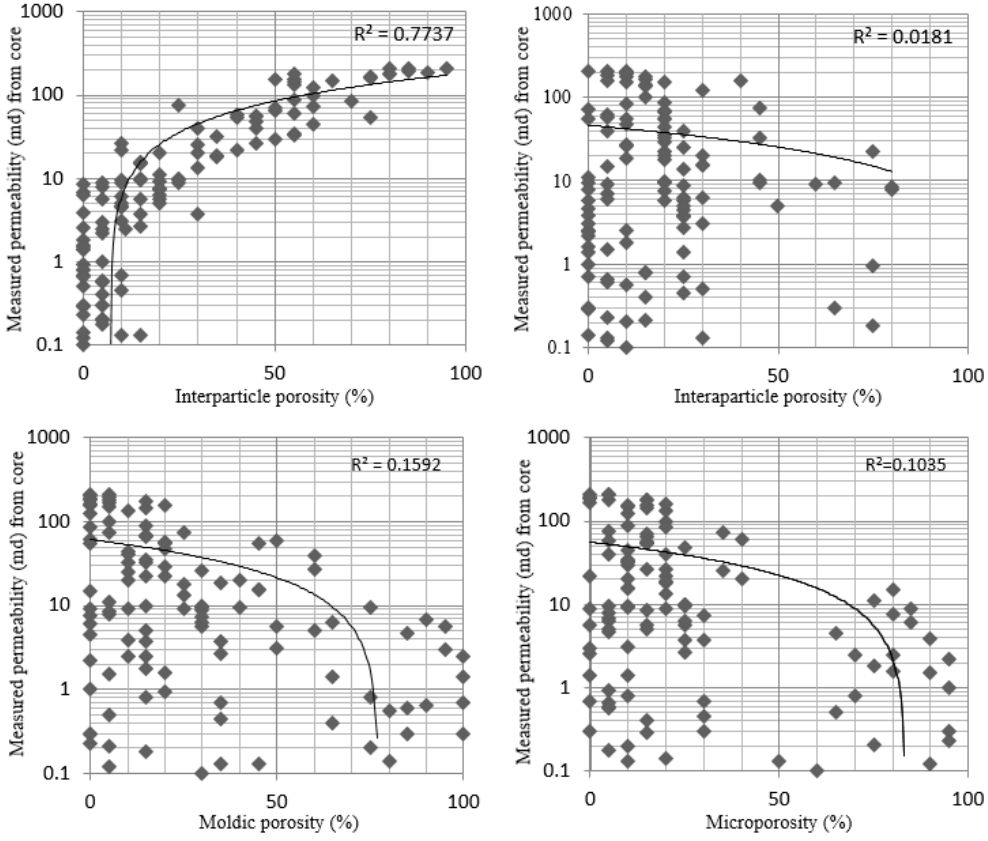

Fig 1. Cross plots show the relationship between the permeability of core and the petrographic data

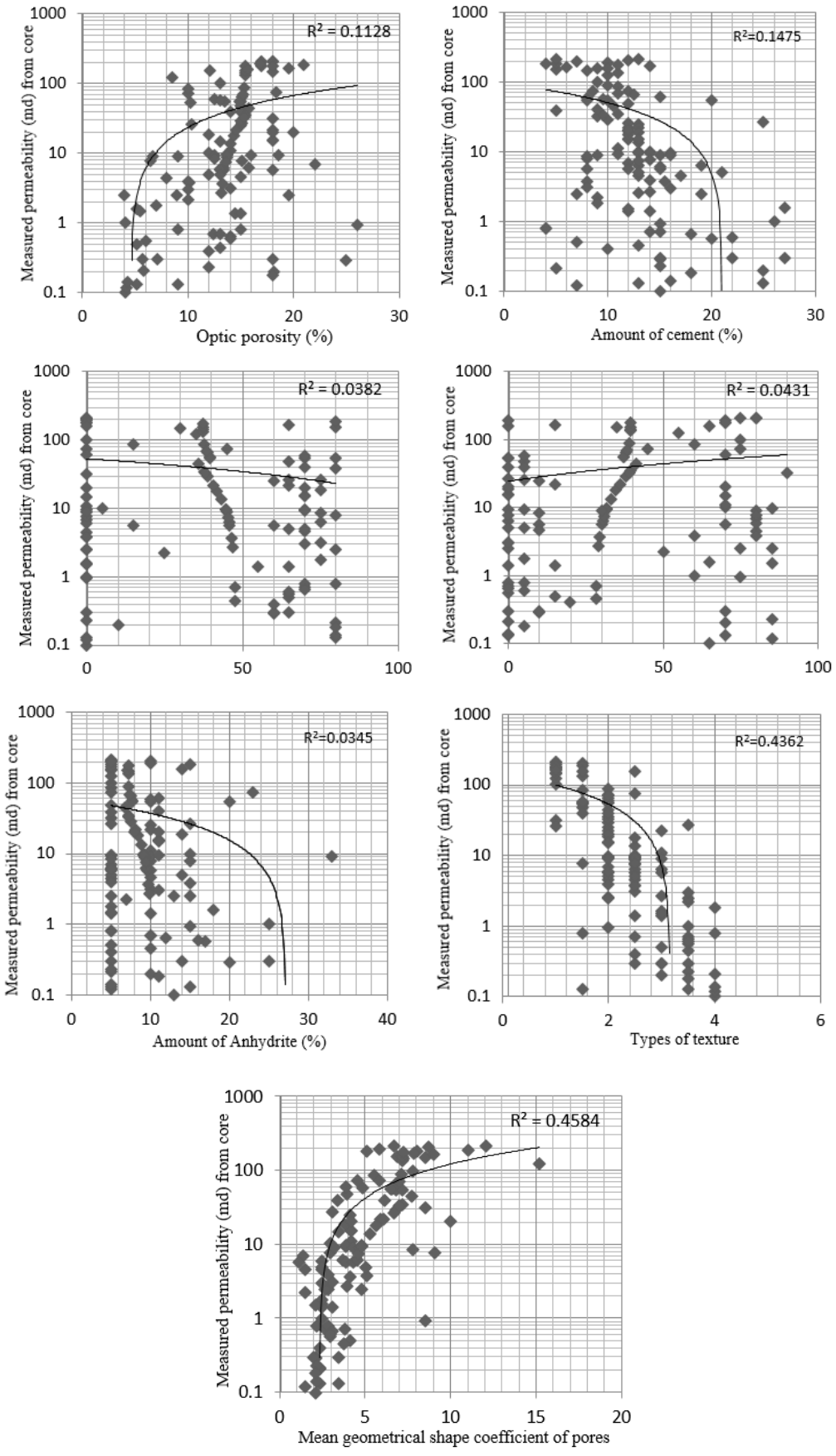

Fig 1. (Continues)

Table 1. The correlation matrix of petrographic features and permeability. F1: intergranular porosity, F2: intragranular porosity, F3: moldic porosity, F4: micro porosity, F5: optical porosity, F6: amount of cement, F7: amount of calcite, F8: amount of dolomite, F9: amount of anhydrite, F10: types of texture, F11: mean geometrical shape coefficient

	F1	F2	F3	F4	F5	F6	F7	F8	F9	F10	F11	K
F1	1											
F2	-0.1369	1										
F3	-0.4787	-0.2331	1									
F4	-0.3438	-0.3066	-0.4425	1								
F5	0.3185	0.1697	0.2037	-0.6283	1							
F6	-0.4018	-0.0528	0.3058	0.0927	-0.2110	1						
F7	-0.1792	0.2247	0.3569	-0.3499	0.0459	-0.0190	1					
F8	0.1863	-0.1733	-0.3719	0.3264	-0.0199	-0.0388	-0.9716	1				
F9	-0.1579	-0.0500	0.0170	0.1643	-0.1730	0.4678	-0.1819	0.0361	1			
F10	-0.7313	-0.0079	0.2575	0.4210	-0.4536	0.3390	0.1811	-0.1892	0.1667	1		
F11	0.7382	0.2435	-0.4645	-0.3736	0.3514	-0.3422	-0.0719	0.1067	-0.1913	-0.6595	1	
K	0.8796	-0.1346	-0.3990	-0.3217	0.3358	-0.3841	-0.1954	0.2076	-0.1858	-0.6605	0.6771	1

Table 2. Characterization of an NN model

Network architecture	Feed forward
Training function	Levenberg-Marquardt backpropagation
Number of layers	3
Number of hidden layers	1
Performance function	MSE
Transfer function between first and second layer	Log sigmoid
Transfer function between second and third layer	Purelin

After training the network, the test data was introduced to the model and the permeability was calculated. The mean squared error (MSE) for the training and test data is equal to 0.0078 and 0.0107, respectively. Fig. 2 shows the relationship between the real and NN permeability values in the test data.

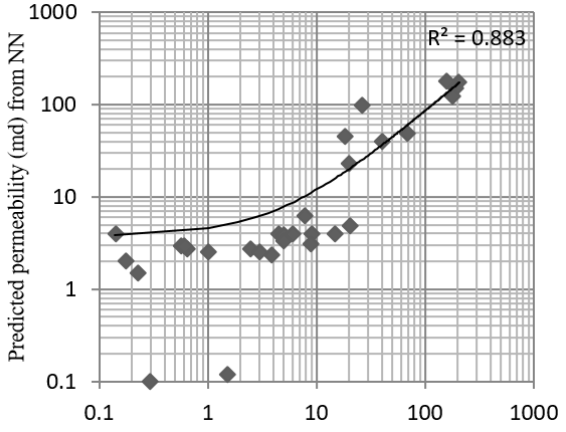

Fig. 2. Cross plot showing the relationship between the measured and NN permeability values

5.2. Fuzzy Logic

A TS-FIS* was employed to predict the permeability. A subtractive clustering method was used for classifying the datasets. The main parameters of the subtractive clustering is determination of the optimal clustering radius. A large clustering radius yields a few large clusters in the data and generates a few rules. Searching for the optimal clustering radius was conducted by repeatedly performing a clustering process and gradually increasing the clustering radius from 0 to 1 (with 0.1 intervals). Therefore, 10 fuzzy models with different numbers of if-then rules were established (Table 3). Then, the fuzzy model with the highest overall accuracy was selected. By specifying the clustering radius of 0.3, the MSE of fuzzy logic (FL) the model becomes minimum. The results show that taking the clustering radius of 0.3 leads to the highest performance. The MSE of the FL for the training and test data is equal to 0.0069 and 0.0081, respectively. Fig. 3. Shows the relationship between the real and FL permeability value in the test data.

Table 3. Clustering radius and MSE for each FL model

o. FIS	MSE of FL model	Clustering radios
1	0.2187	0.1
2	2.71e+16	0.2
3	**0.0069**	**0.3**
4	0.0119	0.4
5	0.0112	0.5
6	0.0111	0.6
7	0.0117	0.7
8	0.0130	0.8
9	0.0128	0.9
10	0.0128	1

5.3. Neuro-fuzzy

Neuro-fuzzy (NF) hybrid systems possess the advantages of fuzzy and neural networks. The process of determining the optimum clustering radius is similar to that of the FL. By specifying the clustering radius of 0.3, the MSE of the NF model becomes minimum (Table 4). The NF was trained by using the training data with 100 epoch. Then, the test data were introduced to the NF model. The MSE of the NF system for the training and test data is equal to 0.0050 and 0.0080, respectively. Fig. 4

* Takagi Sugeno-Fuzzy inference system

shows the relationship between the real and NF permeability values in the test data.

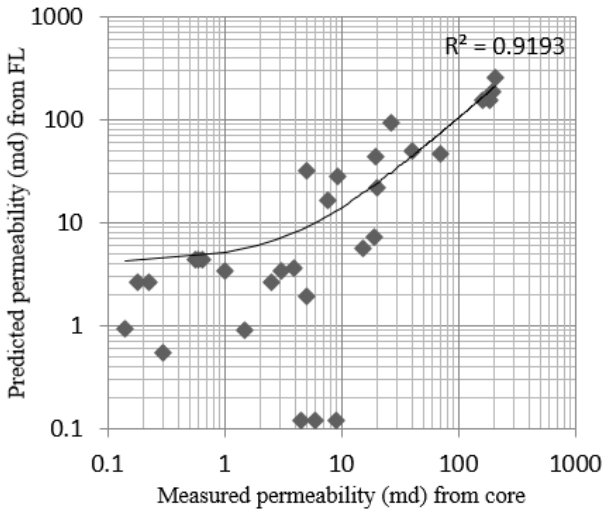

Fig. 3. Cross plot showing the relationship between measured and FL permeability

Table 4. Clustering radius and MSE for each NF model

No. FIS	MSE of FL model	Clustering radios
1	0.0895	0.1
2	2.33e+14	0.2
3	**0.0050**	**0.3**
4	0.0081	0.4
5	0.0072	0.5
6	0.0074	0.6
7	0.0083	0.7
8	0.0110	0.8
9	0.0110	0.9
10	0.0119	1

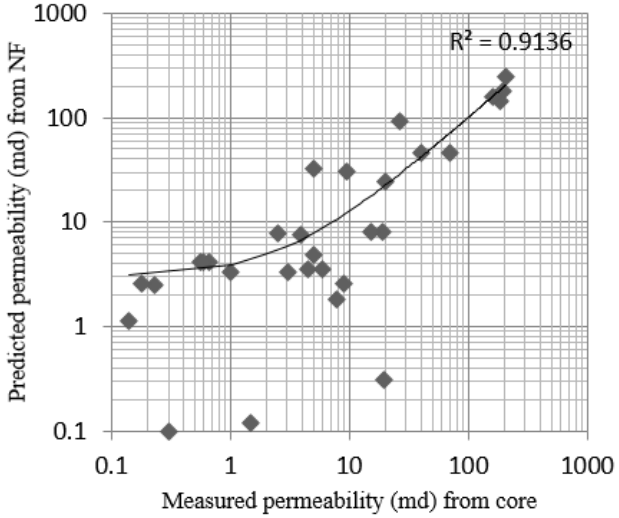

Fig. 4. Cross plot showing the relationship between the measured and NF permeability

5.4. Committee machine with intelligent systems

The committee machine with intelligent systems (CMIS) was constructed in two ways: simple averaging (SA), weighted averaging (WA).

In the CMIS-SA model, each single expert has an equal contribution in constructing the CMIS. A simple computation was carried out according to equation (4).

$$K_{CMIS-SA} = \frac{1}{3}(K_{NN} + K_{FL} + K_{NF}) \quad (4)$$

The MSE of the CMIS-SA model is 0.0072. Therefore, the performance of the predicted model was improved (fig. 5).

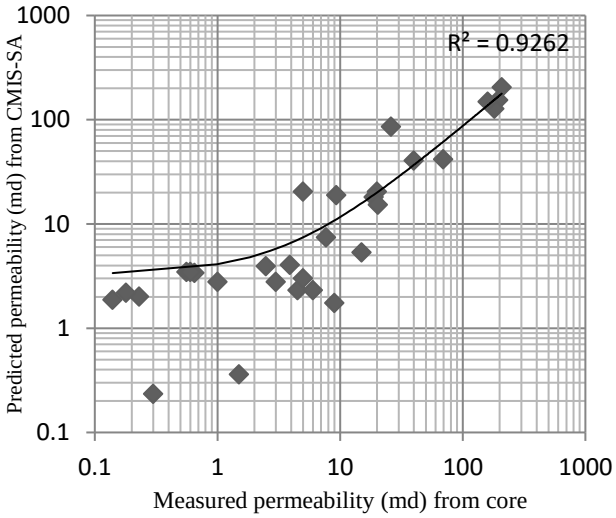

Fig. 5. Cross plot showing the relationship between measured and CMIS-SA permeability

In the CMIS-WA method, a CMIS was constructed using PSO to determine the optimal contribution of the individual intelligent systems. The fitness function should be optimized with PSO according to equation (5).

$$MSE = \frac{1}{n}\sum_{i=1}^{n}(W_1 \times NN_i + W_2 \times FL_i + W_3 \times NF_i) \quad (5)$$

Equation (5) shows the MSE of the CMIS prediction where W_1, W_2 and W_3 weight factors correspond to the predicted permeability from NN, FL and NF, respectively. K_i is the measured permeability from the core plugs and n is the number of training data.

$$K_{CMIS-WA} = 0.2947 \times K_{NN} + 0.3198 \times K_{FL} + 0.4000 \times K_{NF} \quad (6)$$

The MSE of the CMIS-WA model is 0.0066 that shows the minimum MSE with respect to other models. Fig. 6 shows the relationship between the measured and CMIS-WA permeability values in the test data.

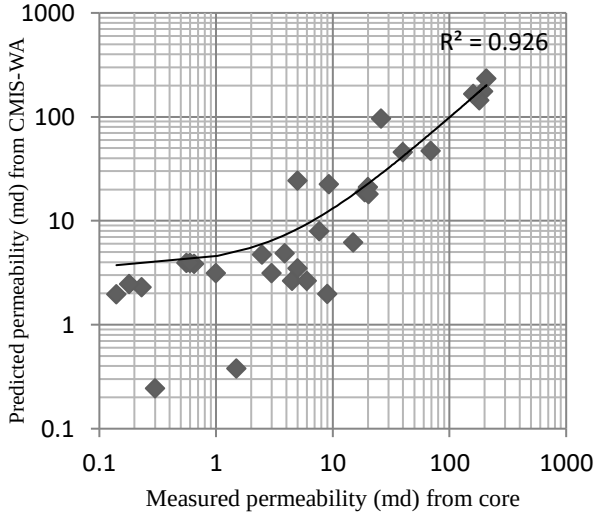

Fig. 6. Cross plot showing the relationship between the measured and CMIS-WA permeability values.

5.5. Multiple linear regression

The MLR was used to explain the relationship between the core permeability as the response variable, and two or more predictor variables. The interparticle porosity (IP), mean geometrical shape coefficient (GSC) and types of texture (T) were considered as the predictor variables. Equation (7) shows the MLR model for permeability prediction.

$$K_{MLR} = 1.5450 \times IP - 3.9641 \times GSC + 3.5690 - 11.0384 \quad (7)$$

Fig. 7 shows the relationship between the measured and MLR results. The correlation coefficient between the measured and MLR permeability is 0.8699.

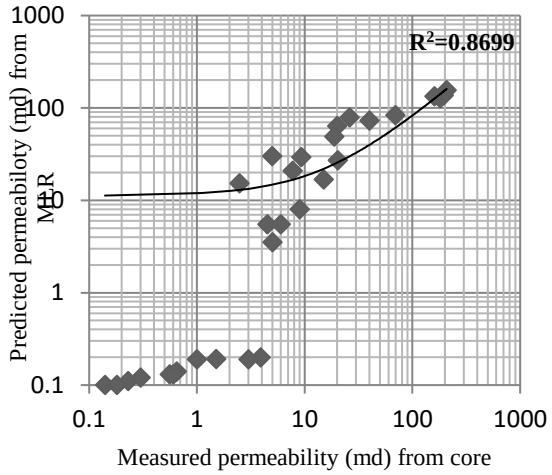

Fig 7. Cross plot showing the relationship between the measured and MLR permeability values.

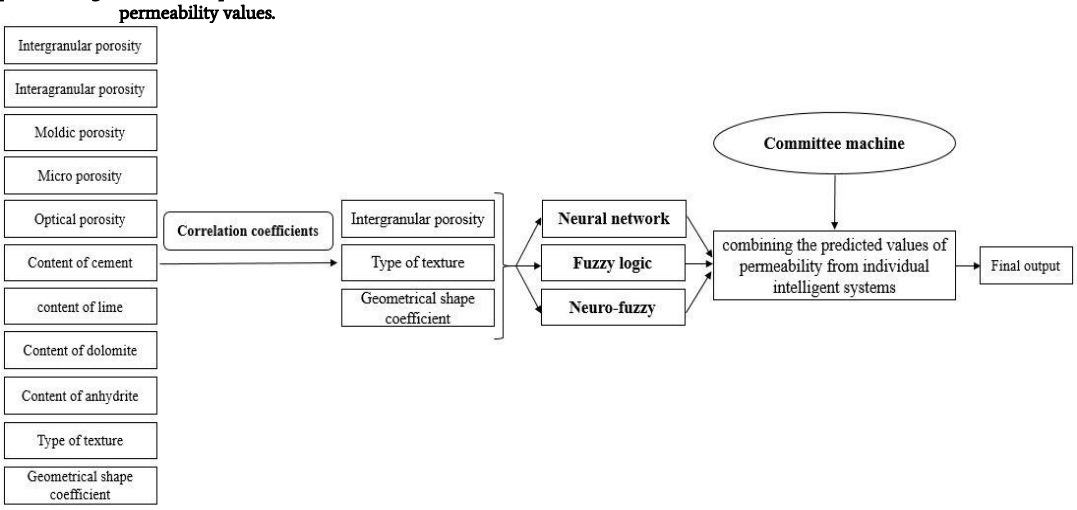

Fig. 8. Graphical representation of workflow

The MLR analysis was used to predict the permeability. MLR attempts to model the relationship between the selected petrographic parameters as explanatory variables and the core permeability as the response variables by fitting a linear equation to the data. The R2 values between the core and MLR permeability are 0.8699. The comparison between the results shows that the intelligent systems have a better performance than the MLR.

This study shows an acceptable prediction of permeability from the petrographic data using various intelligent systems and committee machines.

Using the integration of intelligent systems and the petrographic data can be useful for estimation of permeability, especially in old fields where the cores may be unavailable or are not well preserved. On the other hand, this technique can be applied on the petrographic data collected from drill cutting.

6. Discussion and Conclusion

Image analysis methods applied on thin sections of reservoir rocks, are fast and low cost techniques for predicting the physical properties such as permeability, from solely the knowledge of a porous microstructure of a reservoir rock [48].

A cross plot analysis was used to reduce the dimensionality of the inputs. Comparing the results revealed that the interparticle porosity, the mean geometrical shape coefficient, and the type of texture from the petrographic data have a stronger relationship with the permeability. Therefore, these parameters were selected as inputs of the intelligent models. Fig. 8 shows a graphical representation of the workflow.

The selected petrographic features were used as inputs of the NN, FL and NF models. The MSE of the NN, FL and NF models for prediction of the permeability in the test data are 0.0107, 0.0081 and 0.0080, which correspond to R^2 values of 0.8830, 0.9193 and 0.9136, respectively.

The concept of CMIS was used to combine and improve the results of the NN, FL and NF models. Two kinds of CMISs were applied: CMIS-SA and CMIS-WA. The CMIS-WA was carried out to obtain the optimal combination of the weights using a PSO algorithm. The derived weights from the PSO algorithm for the NN, FL and NF models are 0.2947, 0.3198 and 0.4000, respectively. The MSE of CMIS-SA and CMIS-WA for the test data are 0.0072 and 0.0066, which correspond to R^2 values of 0.9262 and 0.9260, respectively.

The models' MSE values show accurate predictions of the permeability. In addition, the correlation coefficients between the predicted permeability from the models and the core permeability support this fact. Furthermore, it is clear that the CMIS-SA and CMIS-WA perform better than the NN. FL and NF models.

Acknowledgement

The authors would like to thank the Shahrood University of Technology and the Iranian Central Oil Fields Company (ICOFC) for providing with the technical supports and industrial engineering consideration, respectively. In addition, helpful revisions and suggestions of two anonymous referees of the International Journal of Mining and Geo-Engineering are kindly acknowledged.

REFRENCES

[1]- Mohaghegh, S., Arefi, R., Ameri, S., & Hefner, M. H. (1994). A methodological approach for reservoir heterogeneity characterization using artificial neural networks. *SPE annual technical conference and exhibition*, 1-5.

[2]- Huang, Y., Gedeon, T.D., & Wong, P. M. (2001). An integrated neural-fuzzy-genetic-algorithm using hyper-surface membership functions to predict permeability in petroleum reservoirs. *Engineering Applications of Artificial Intelligence*, 14(1), 15-21.

[3]- Lim, J. S. (2005). Reservoir properties determination using fuzzy logic and neural networks from well data in offshore Korea. *Journal of Petroleum Science and Engineering*, 49(3), 182-192.

[4]- Kazem Shiroodi, S., Ghafoori, M., & Khanian, M. (2012). Secondary porosity index effect on improving permeability estimation from petrophysical logs utilizing artificial intelligent approaches. *Iranian Journal of Petroleum Geology*, 3(3), 77-98.

[5]- Rafik, B. & Kamel, B. (2016). Prediction of permeability and porosity from well log data using the nonparametric regression with multivariate analysis and neural network, Hassi R'Mel Field, Algeria. *Egyptian Journal of Petroleum*, 1-16

[6]- Berryman, J. G., & Blair, S. C. (1986). Use of digital image analysis to estimate fluid permeability of porous materials: Application of two-point correlation functions. *Journal of Applied Physics*, 60(6), 1930-1938.

[7]- Blair, S. C., Berge, P. A. & Berryman, J. G. (1996). Using two-point correlation functions to characterize microgeometry and estimate permeabilities of sandstones and porous glass. *Journal of Geophysical Research: Solid Earth (1978–2012)*, 101(B9), 20359-20375.

[8]- Solymar, M., & Fabricius, I. L. (1999). Image analysis and estimation of porosity and permeability of arnager greensand, Upper cretaceous, Denmark. *Physics and Chemistry of the Earth, Part A: Solid Earth and Geodesy*, 24(7), 587-591.

[9]- Tiab, D., & Donaldson, E. C. (2004). Theory and practice of measuring reservoir rock and fluid transport properties. Gulf professional publishing, 100-105.

[10]-Winardhi, C. W., Maulana, F. I., & Latief, F. D. E. (2016). Permeability estimation of porous rock by means of fluid flow simulation and digital image analysis. *IOP Conference Series: Earth and Environmental Science*, 29(1), 1-6.

[11]- Coskun, S. B., & Wardlaw, N. C. (1993). Estimation of permeability from image analysis of reservoir sandstones. *Journal of Petroleum Science and Engineering*, 10(1), 1-16.

[12]- Anselmetti, F. S., Luthi, S., & Eberli, G. P. (1998). Quantitative characterization of carbonate pore systems by digital image analysis. *AAPG Bulletin*, 82(10), 1815-1836.

[13]- Ali, M., & Chawathé, A. (2000). Using artificial intelligence to predict permeability from petrographic data. *Computers and Geosciences*, 26(8), 915-925.

[14]- Egmont-Petersen, M., de Ridder, D., & Handels, H. (2002). Image processing with neural networks—A Review. *Pattern Recognition*, 35(10), 2279-2301.

[15]- Garnham, J., & Hatfield, K. (2001). The Application of image analysis to improve permeability prediction, *Petrophysics*, 42(05), 457-467.

[16]- Lock, P. A., Jing, X., Zimmerman, R. W., & Schlueter, E. M. (2002). Predicting the permeability of sandstone from image analysis of pore structure. *Journal of Applied Physics*, 92(10), 6311-6319.

[17]- Zimmerman, R. W., Jing, X., Lock, P. A., and Jurgawczynski, M. (2007). Permeability predictions based on two-dimensional pore space images. *SPE Annual Technical Conference and Exhibition*, 1-10.

[18]- Wieling, I. S. (2013). Facies and permeability prediction based on analysis of core images, Delft University of Technology, 1-141.

[19]- Blunt, M.J., Bijeljic, B., Dong, H., Gharbi, O., Iglauer, S., Mostaghimi, P., Paluszny, A., & Pentland, C. (2013). Pore-scale imaging and modelling. *Advances in Water Resources*, 51, 97-216.

[20]-Saxena, N., Mavko, G., Hofmann, R., & Srisutthiyakorn, N. (2017). Estimating permeability from thin sections without reconstruction: Digital rock study of 3D properties from 2D images. *Computers & Geosciences*, 102, 79-99.

[21]- Haykin, S., & Lippmann, R. (1994). Neural networks, a comprehensive foundation. *International Journal of Neural Systems*, 5(4), 363-364.

[22]- Sharkey, A. J. C. (1996). On combining artificial neural nets. *Connection Science*, 8(3-4), 299-314.

[23]- Kadkhodaie-Ilkhchi, A., Rahimpour-Bonab, H., & Rezaee, M. (2009). A committee machine with intelligent systems for estimation of total organic carbon content from petrophysical data: an example from kangan and dalan reservoirs in South Pars Gas Field, Iran. *Computers & Geosciences*, 35(3), 459-474.

[24]- Labani, M. M., Kadkhodaie-Ilkhchi, A., & Salahshoor, K. (2010). Estimation of NMR log parameters from conventional well log data using a committee machine with intelligent systems: A case study from the Iranian part of the South Pars Gas Field, Persian Gulf Basin. *Journal of Petroleum Science and Engineering*, 72(1), 175-185.

[25]- Sadeghi, R., Kadkhodaie, A., Rafiei, B., Yosefpour, M., & Khodabakhsh, S. (2011). A committee machine approach for predicting permeability from well log data: a case study from a heterogeneous carbonate reservoir, Balal oil Field, Persian Gulf. *JGeope*, 1(2), 1-10.

[26]- Hatampour, A. (2013). Developing a committee machine model for Predicting reservoir porosity from image analysis of thin sections. *Middle-East Journal of Scientific Research*, 13(11), 1438-1444.

[27]- Rostami, A., Hatampour, A., Amiri, M., Ghiasi-Freez, J., and Heidari, M. (2014). Developing a committee machine model for predicting reservoir porosity from image analysis of thin sections, *20th Formation Evaluation Symposium of Japan*, 1-10.

[28]- Shokrollahi, A., Tatar, A., & Safari, H. (2015). On accurate determination of PVT properties in crude oil systems: committee machine intelligent system modeling approach. *Journal of the Taiwan Institute of Chemical Engineers*, 55, 17-26.

[29]- Ghiasi-Freez, J., Kadkhodaie-Ilkhchi, A., & Ziaii, M. (2012). Improving the accuracy of flow units prediction through two committee machine models: an example from the South Pars Gas Field, Persian Gulf Basin, Iran. *Computers & Geosciences*, 46, 10-23.

[30]- Eberhart, R. C., & Hu, X. (1999). Human tremor analysis using particle swarm optimization. *Evolutionary Computation*, 3, 1927-1930.

[31]- Parsopoulos, K. E. ed. (2010). Particle swarm optimization and intelligence: advances and applications. IGI Global.

[32]- Yan, X., Zhang, C., Luo, W., Li, W., Chen, W., & Liu, H. (2012). Solve traveling salesman problem using particle swarm optimization algorithm. *International Journal of Computer Science*, 9, 264-271.

[33]- Kung, C. C., & Chen, K. Y. (2013). Missile guidance algorithm design using particle swarm optimization. *Applied Mechanics and Materials*, 284, 2411-2415.

[34]- Shi, Y., & Eberhart, R. C. (1999). Empirical study of particle swarm optimization. *Evolutionary Computation*, 3, 1945-1950.

[35]- Coello, C. A. C., Pulido, G. T., & Lechuga, M. S. (2004). Handling multiple objectives with particle swarm optimization. *Journal of IEEE Transactions on Evolutionary Computation*, 8(3), 256-279.

[36]- Poli, R., Kennedy, J., & Blackwell, T. (2007). Particle swarm optimization. *Swarm intelligence*, 1(1), 33-57.

[37]-Ali Ahmadi, M., Zendehboudi, S., Lohi, A., Elkamel, A., & Chatzis, I. (2013). Reservoir permeability prediction by neural networks combined with hybrid genetic algorithm and particle swarm optimization. *Geophysical Prospecting*, 61(3), 582-598.

[38]- Kiany, D., (2017), "Iran and Qatar, gas production in South Pars",

Palma Journal, 16, pp. 150-159.

[39]- Aali, J., Rahimpour-Bonab, H., & Kamali, M. R. (2006). Geochemistry and origin of the world's largest gas field from Persian Gulf, Iran. *Journal of Petroleum Science and Engineering*, 50(3), 161-175.

[40]- Gonzalez, R. C., & Woods, R. E. (2006). Digital Image Processing. Third edition, Prentice hall publishing, Pearson education, 465-468.

[41]- Bhatt, A., & Helle, H. B. (2002). Committee neural networks for porosity and permeability prediction from well logs. *Geophysical Prospecting*, 50(6), 645-660.

[42]- Zadeh, L. A. (1965). Fuzzy sets. *Information and Control*, 8(3), 338-353.

[43]- Mamdani, E. H., & Assilian, S. (1975). An experiment in linguistic synthesis with a fuzzy logic controller. *International Journal of Man-machine Studies*, 7(1), 1-13.

[44]- Takagi, T., & Sugeno, M. (1985). Fuzzy identification of systems and its applications to modeling and control. *IEEE Transactions on Systems, Man, and Cybernetics*, (1), 116-132.

[45]- Kennedy, J., & Eberhart, R. (1995). Particle swarm optimization. *1995 IEEE international conference on neural networks*, 1942-1948.

[46]- Matthews, D. E. (2005). Multiple linear regression. In: Encyclopedia of biostatistics, second edition, Armitage, P. & Colton, T. (eds.), John Wiley and sons, 3428-3441.

[47]- Hudson Beale, M., Hagan, M. T. and Demuth, H. B. (2017). Matlab user's Guide: Neural Network Toolbox. Mathwork Inc., 2-3.

[48]- Philippi, P. C., Damiani, M. C., Fernandes, C. P., Bueno, A. D., Santos, L. O. E., & da Cunha Neto, J. A. B., (2000). Characterization of reservoir rocks from image analysis on imago software. *Workshop-RECOPE*, 1-5.